Applied Thermal Engineering 242 (2024) 122485

Contents lists available at ScienceDirect

Applied Thermal Engineering

journal homepage: www.elsevier.com/locate/apthermeng

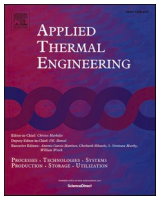

Research Paper

Solar driven liquid desiccant dehumidification system: Measurements and annual system simulations

Wael Mandow, Felix Micus, Lisa Völker *, Daniel Fleig, Ulrike Jordan

Institute of Thermal Engineering, University of Kassel, Kurt-Wolters-Str. 3, 34125 Kassel, Germany

ARTICLE INFO

Keywords:
Liquid desiccant
Dehumidification
Regeneration
Solar heat
TRNSYS

ABSTRACT

Liquid desiccant air conditioning (LDAC) systems are used for dehumidification of air to low dew point temperatures. In the presented study a TRNSYS model of a LDAC unit is developed and validated with laboratory measurements. This model is coupled with a solar thermal system that provides heating water for the regeneration process. With this model dynamic annual system simulations can be carried out to simulate the dehumidification of a building. The solar fraction is evaluated for various infiltration rates of the building and solar collector areas with an internally cooled as well as an adiabatic absorption process.

The simulation results reveal that high solar fractions of 70 % to 81 % can be achieved when dimensioning the solar thermal system to cover the regeneration heat demand on a good summer day. This is due to the good correlation of solar irradiance and dehumidification load. Without internal cooling of the absorption process (adiabatic conditions), the solar fraction is reduced by about 10 percent points for the same size and operating conditions.

1. Introduction

Liquid desiccant air conditioning (LDAC) systems are used for air dehumidification. The systems reach a low humidity ratio of the supply air and they aim to reduce electrical energy consumption if they replace vapor compression systems. In the recent years, LDAC systems attract more and more attention. The systems consist essentially of an absorber, a regenerator, as well as an internal heat exchanger for the liquid desiccant and a desiccant storage.

LDAC systems can usually be operated with low-grade heat with regeneration temperatures of about 60–80 °C (e. g. [1,2]). In addition, dehumidification demand correlates to thermal solar energy supply. As a result, the electricity consumption for room air dehumidification with LDAC systems can be significantly reduced by using solar energy or waste heat compared to vapor compression systems (e. g. [3,4]). Furthermore, the LDAC system can guarantee better hygienic indoor air quality in comparison to vapor compression systems by avoiding bacteria and germs and separating foreign bodies ([5,6]). LDAC systems were tested for drying applications of agricultural goods such as hay bales [7], tea [8] or grain [9]. In comparison to conventional drying processes with hot air, the studies show a shorter drying time, cost savings and a better quality of the drying goods. Kozubal et al. [4] install and examine four LDAC systems in the USA to dehumidify room air (in supermarkets, a swimming pool and a campus building). The LDAC systems provide a relative humidity in the buildings of 35–55 % and could reduce the electricity consumption by more than 50 % in these pilot systems compared to conventional vapor compression systems.

To investigate the performance of the LDAC systems under different weather conditions as well as use cases, many LDAC system models were developed like [4,10,11,12,13] and [14]. The developed model by [10] was used to develop a model of an existing solar driven LDAC system. The model of [10] was used to investigate the performance of the LDAC system for three options of solar collector designs for three cities [15]. The building was not modeled by [15]. By [11] the building is represented by a previously derived cooling demand and then simulated with an LDAC system for three days. The system models by [4] and [10] include, contrary to the other mentioned systems, component models for the absorber, the regenerator as well as the desiccant sump. Crofoot [10] models the desiccant sump as a single-chamber storage with a homogeneous temperature and a homogeneous mass fraction. Kozubal et al. [4] models two separate desiccant chambers (for concentrated and diluted solution) with stratification and possible mixing. Regarding the absorber and regenerator component models used in the developed LDAC system models, the absorber and regenerator model by Mohaisen and Ma [11] only describes the adiabatic process, while all other

* Corresponding author.
E-mail address: solar@uni-kassel.de (L. Völker).

https://doi.org/10.1016/j.applthermaleng.2024.122485
Received 9 October 2023; Received in revised form 22 December 2023; Accepted 15 January 2024
Available online 17 January 2024

Nomenclature

A	Area, m^2
AAD	Average absolute deviation
AAD%	Percentage average abs. deviation, %
c_i	Maximum mass transfer potential ratio
c_p	Specific heat capacity, J/kgK
D	Diffusion coefficient, m^2/s
f_{solar}	Solar fraction
$\dot{H}_{sorp.}$	Sorption enthalpy flow, W
Le	Lewis number
m	Mass, kg
$\dot{m}$	Mass flow rate, kg/s
n	Number of samples
n_{inf}	Infiltration rate, h^{-1}
NTU	Number of transfer units
Q	Thermal energy, J; kWh
$\dot{Q}$	Heat flow rate, W
q_{coll}	Specific solar yield, kWh/m^2
RSHI	Regenerator specific heat input, J/kg_w
t	Time, h
T	Temperature, °C
ΔT	Temperature difference, K
U	Thermal transmittance, W/m^2K
V	Volume, m^3
x	Humidity ratio, kg_w/kg_{da}
X	Water content in salt, kg_w/kg_{LiCl}

Subscripts

a	Air
abs	Absorber
amb	Ambient
aux	Auxiliary heater
coll	Collector
da	Dry air
eq	Equilibrium
in	Inlet
inf	Infiltration
meas	Measurement
out	Outlet
reg	Regenerator
salt	Salt (LiCl)
sens	Sensible
set	Setpoint
sim	Simulation
sol	Liquid desiccant solution
sorp	Sorption
st	Storage tank
v	Water vapour
w	Cooling or heating water

Greek symbols

α	Heat transfer coefficient, W/m^2K
β	Mass transfer coefficient, kg/m^2s
ε	Effectiveness
κ_e	Energy balance factor
κ_m	Mass balance factor
λ	Thermal conductivity, W/mK
ξ	Mass fraction, kg_{LiCl}/kg_{sol}
ρ	Density, kg/m^3

Abbreviations

LDAC	Liquid desiccant air conditioning
Nu	Nusselt

mentioned models describe internally cooled and internally heated processes.

Kozubal et al. [4] developed physical and empirical component models for the absorber and regenerator, which were then used to derive performance maps used for the LDAC system model. Crofoot [10] as well as Mohaisen and Ma [11] used simplified ε-NTU correlations for the absorber as well as regenerator model. Zhang et al. [12] as well as Yang et al. [13] based the absorber as well as regenerator models on NTU-Le correlations. In the models by [10] and [11] the effectiveness of the heat and mass transfer is determined on the basis of correlations depending on boundary conditions. The models by [10,4] and [11] are suitable to describe transient conditions while the models by [12] and [13] are only applicable for stationary conditions.

The LDAC system model by Crofoot [10] includes a desiccant sump that is based on empirical heat and mass transfer coefficients evaluated for that system and is validated based on their own measurements for transient ambient conditions. The study presents six-hour measurement data with an average absolute deviation between the measured and calculated humidity ratio of 2 %. The average absolute deviation of the moisture removal rate for three days system measurements is reported as 6, 10 and 8 %, for each of the days. There is no information about the validation of the regeneration process [10]. Mohaisen and Ma [11] validated the component models of absorber and regenerator, the system model was not validated.

Therewith, there is no system model of an LDAC unit available yet, that is based on equations to model the heat and mass transfer without detailed knowledge of the heat and mass transfer or other performance coefficients in advance and that is also able to model transient system behavior sufficiently.

The inertia of the system to reach the state of equilibrium is influenced strongly not only by the size of the liquid desiccant storage, but also, for example, by the mass flow rates and the design of the absorber and regenerator. The liquid desiccant storage enables the continuous operation of the LDAC unit for practical applications. The overall desiccant concentration will reach a stable point, where continuous operation is possible by matching the water vapor mass flow rate in the regenerator and in the absorber. With the difference in air volume flow rate, it means that the resulting difference between inlet and outlet humidity ratio in the regenerator might differ from the absorber. To accurately reflect this behavior, especially in dynamic conditions, it is necessary to model the liquid desiccant storage as well. Especially the modeling of the liquid desiccant storage with the partial mixing between the diluted and the concentrated liquid desiccant is very important to reach high accuracy by the simulation results.

The developed LDAC model is suitable to conduct dynamic annual system simulations in combination with a solar thermal system. Controllers are employed for the system to dynamically control the set-point humidity in the modeled building by regulating the capacity, controlling the solar loop and activating an auxiliary heater throughout the simulation. Only few annual simulation studies of controlled solar-driven LDAC systems can be found in literature. Coca-Ortegón [14] investigated a solar driven liquid desiccant system using performance tables as input values for the absorber and regenerator which were developed based on measurement data. The solar fraction for their studied system with weather data of Kuala Lumpur is in a range of 42 % to 54 % depending on regeneration temperature and maximum LiCl mass fraction in the desiccant tank. Compared to the system in the present paper, the system of [14] works with constant regeneration temperature and

outlet humidity ratio is not controlled.

In the following section 2, this paper describes the investigated LDAC unit design, followed by a brief description of the component models (section 3). Focus of this study, described in section 4, is the validation of the system model for an LDAC unit with a 6-hour laboratory measurement as well as two 6-day measurements with emulated temperature and humidity outdoor conditions. Finally, dynamic annual system simulation results of the LDAC system including a coupled solar heating system are presented in section 5.

2. Overall LDAC system set-up

The investigated LDAC system includes a solar thermal system for heat supply as well as a cooling tower as shown in Fig. 1 b). The LDAC unit was built by AIL Research, Inc (AILR). It consists of an absorber (dehumidifier), a regenerator, a desiccant sump and an internal heat exchanger of the concentrated and diluted desiccant solution. In the internally cooled absorber and heated regenerator, air passes along a liquid desiccant film in cross flow configuration. In the absorber, water vapor is absorbed by the concentrated aqueous LiCl-solution due to its lower water vapor pressure above the solution compared to that of the air. Enthalpy of absorption (evaporation and dilution) is released during the process and is transferred to the air and liquid desiccant, as well as to the cooling water inside the absorber. The now diluted desiccant solution flows through the internal heat exchanger into the sump before it is concentrated in the regenerator. The absorber and regenerator are made of corrugated fiber glass sheets as wicking fins attached to cupronickel tube bundles, Fig. 1 a). The desiccant sump is composed of a single tank (sump) with coupled areas for diluted and concentrated solutions that are kept apart by the internal solution heat exchanger. In the internal heat exchanger, sensible heat is transferred from the concentrated to the diluted desiccant stream. Entrainment of the desiccant into the air is not investigated. Table 1 shows the specific data of the AILR-LDAC unit.

All relevant in- and outlet parameters of the air, liquid desiccant, and cooling or heating water are measured. Table 2 shows the measurement errors assumed for the analysis, considering both the manufacturer's specifications and estimated errors due to sensor positioning.

Table 1
Specific data of the AILR- LDAC unit.

	Absorber	Regenerator
Air volume flow rates	2000 m^3/h	600 m^3/h
Desiccant mass flow rates	330 kg/h	230 kg/h
Water mass flow rates	2000 kg/h	1000 kg/h
Water inlet temperatures	25 °C	60 °C
Fiberglass surfaces	60 m^2	27 m^2
Tube bundle heat transfer surfaces	2 m^2	1 m^2

Table 2
Estimated measurement accuracies (based on instrument manufacturer's data).

Used measurement technology	Accuracy
Air	
Inlet and outlet temperature	±0.3 K
Inlet and outlet relative humidity	±0.8 % RH (at 10…30 °C) ±1.3 % RH (at 30…60 °C)
Volume flow meter	±1.5 % of reading
Liquid desiccant	
Inlet and outlet temperature	±0.5 K
Inlet density	+0.005 g/cm^3
Mass flow meter	±0.15 % of reading
Cooling/ heating water	
Inlet and outlet temperature	±0.5 K
Mass flow rate	±0.5 % of reading

3. Modelling of LDAC system

A TRNSYS model of the LDAC unit is connected to a solar collector, a water heat storage, a simplified cooling tower and an industrial single zone building model. The respective component models are briefly explained below. The LDAC unit dehumidifies the indoor air continuously by air circulation. A set-point humidity ratio of the indoor air of 6 g_w/kg_{da} was chosen which corresponds to a dew point temperature of 6.6 °C. Those conditions might be required for an application in which condensation on cold piping needs to be avoided, such as pumping stations for fresh water. The moisture entry into the building is varied for different infiltration rates. The latter is varied between 0.1 and 0.7 h^{-1}. Table 3 shows the standard and the self-defined TRNSYS types used in the solar driven LDAC system simulation. The LDAC unit comprises the first four components: absorber, regenerator, desiccant storage and solution pump.

3.1. Absorber and regenerator model

The model of the absorber and regenerator is a single-node ε-NTU model based on efficiency correlations as described in [16]. The temperature and the mass fraction of the desiccant are calculated at the phase boundary with a Newton-Raphson algorithm. The heat of dilution

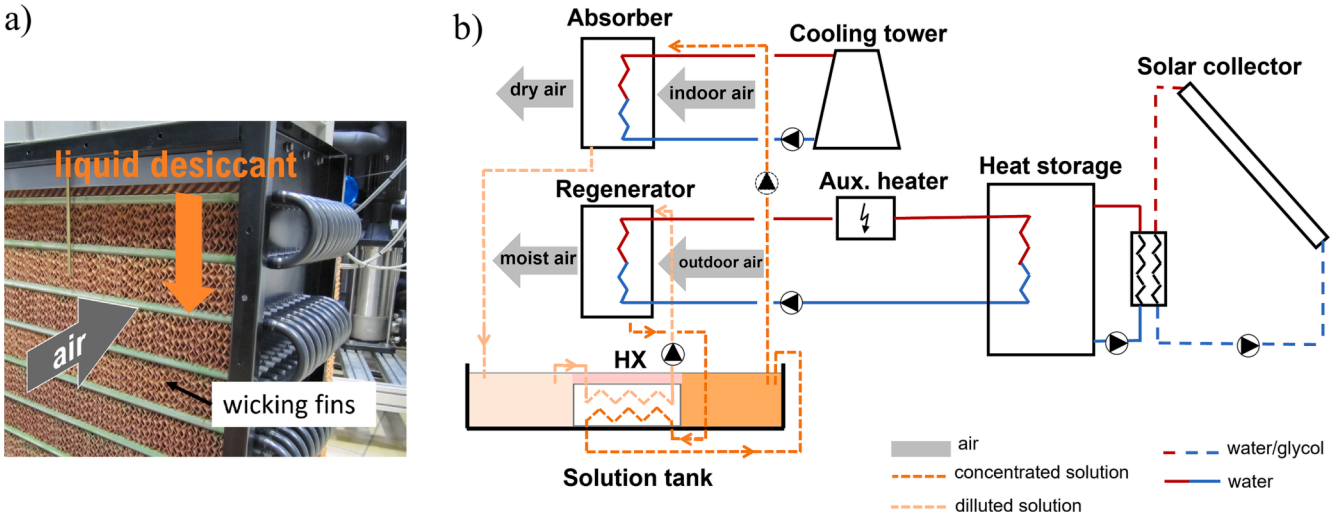

Fig. 1. a) Wicking fins in the absorber and b) regenerator and the LDAC system layout showing the LDAC unit including the solar thermal system and the cooling tower.

Table 3
Standard and self-defined TRNSYS types used in the system simulation.

Component	Type number
Absorber	Custom Type (user-defined)
Regenerator	Custom Type (user -defined)
Desiccant storage (sump)	Custom Type (user-defined)
Solution pump	Type 742
Solar thermal system	Type 832 (collector)
(IEA- SHC-Task 32) [13]	Type 140 (DHW-tank)
	Type 5 (Heat Exchanger)
	Type 3 (Water/Glycol Pump)
Weather data	Type 109-TMY2
Building	Type 56
Auxiliary flow-through heater	Type 6
Differential Controller with Hysteresis	Type 2
PID Controller	Type 23

and vapor pressure correlations are implemented as nonlinear correlations of temperature and mass fraction according to Conde [17]. The heat transfer coefficients and the efficiency of the heat transfer are calculated with correlations according to [18], whereas the heat transfer coefficient of water in the tubes is calculated based on Nu-correlation for flow-through pipes, the heat transfer coefficient of air is based on Nu-correlation for flow in plane gap and the heat transfer coefficient of the desiccant is based on Nu-correlation for cross-flow pipe bundles.

The Lewis number (Le) is calculated from air properties as a function of its temperature and humidity ratio (eq. (1)). Finally, the mass transfer coefficient (β_a) and the efficiency of the mass transfer is calculated in a similar way as the parameters of the heat transfer (eq. (2)). The NTU_β for the mass transfer is given by (eq. (3)).

$$\mathrm{Le} = \frac{\lambda_a}{D_a \cdot c_p \cdot \rho_a} \tag{1}$$

$$\beta_a = \frac{\alpha_a \cdot D_a}{\lambda_a} \cdot Le^{\frac{1}{3}} \tag{2}$$

$$\mathrm{NTU}_\beta = \frac{\beta_a \cdot A}{\dot{m}_{da}} \tag{3}$$

The wicking fins (Fig. 1) are considered simplified as flat plates with a distance of 3 mm between the plates. The heat and mass transfer area between air and desiccant is assumed to be equal to the total plate surface. The heat transfer area between desiccant and cooling/heating water is assumed to be equal to the tube bundle surface. The effectiveness of heat transfer between desiccant interface and air $\varepsilon_{\alpha,a-sol}$ as well as cooling or heating water $\varepsilon_{UA,w-sol}$ depends on the dimensionless number of transfer units NTU_a and NTU_w as given in eq. (4) and eq. (5) according to [18]:

$$\varepsilon_{\alpha,a-sol} = 1 - \exp(-\mathrm{NTU}_a) = 1 - \exp\left(-\frac{\alpha A_a}{c_{p,a}\dot{m}_a}\right) \tag{4}$$

$$\varepsilon_{UA,w-sol} = 1 - \exp(-\mathrm{NTU}_w) = 1 - \exp\left(-\frac{UA_w}{c_{p,w}\dot{m}_w}\right) \tag{5}$$

The effectiveness of the mass transfer process for crossflow configuration is calculated analogous to the heat transfer with eq. (6) and eq. (7) according to [18]:

$$\varepsilon_{\beta,a-sol} = \frac{1}{c_i \cdot \mathrm{NTU}_{\beta i}} \cdot \sum_{m=0}^{\infty} \left\{ \left[1 - \exp(-\mathrm{NTU}_{\beta i}) \cdot \sum_{j=0}^{m} \frac{1}{j!} \mathrm{NTU}_{\beta i}^{j} \right] \cdot \left[1 - \exp(-c_i \mathrm{NTU}_{\beta i}) \cdot \sum_{j=0}^{m} \frac{1}{j!} (c_i \cdot \mathrm{NTU}_{\beta i})^{j} \right] \right\} \tag{6}$$

$$c_i = \frac{\dot{m}_{salt} \cdot (X_{eq} - X_{in})}{\dot{m}_{da} \cdot (x_{a,in} - x_{a,eq})} \tag{7}$$

For the TRNSYS model of the absorber and regenerator following geometrical data has to be defined: number of gaps (between the plates) and the gap width, height and width of plate, plate thickness, outer and inner tube diameter, amount of vertical and horizontal tubes, length of single tube, distance between single tubes (horizontal and vertical) and the cross-division ratios of the pipes.

The absorber and regenerator model were validated with laboratory measurements for a wide range of the inlet parameters for the absorption and regeneration process [16]. These included variations of heating and cooling water temperature and mass flow rate, the humidity ratio of the inlet air, the air mass flow rate at absorber inlet, and the desiccant mass flow rate.

3.2. Desiccant sump and heat exchanger model

Each storage tank of the desiccant sump is described as single-node model with homogeneous temperature and water mass fraction. If the desiccant mass flow rate through the absorber is higher than the desiccant mass flow rate through the regenerator, part of the diluted desiccant solution flows into the other tank and is mixed with the concentrated solution. The used internal solution counter flow heat exchanger model is a standard TRNSYS type. The overall heat transfer coefficient multiplied with the heat transfer surface (UA) of the solution heat exchanger was estimated from the experimental data and was assumed to be equal for all simulations ($UA = 500$ W/K).

3.3. Building model

The building model is developed with TRNBuild. It is a single zone model with a volume of 1000 m^3. Indoor air is circulated and dehumidified with the LDAC unit. The location for the weather data used is Kassel, Germany. The humidity load is solely caused by infiltration, with varying infiltration rates. Other factors of the building like the wall constructions and radiation through windows have little influence on the performance of the dehumidification system. This was confirmed by simulations with different building types. For the study a building with a footprint of 200 m^2, a total exterior shell area of 850 m^2 and U-values of 0.193 W/(m^2K), which corresponds to a *KfW-40* standard of the *German Energy Act for Buildings*,[1] is used. The building type is a standard TRNSYS component, the energy as well as the moisture balance both match. Therefore, the accuracy of modeling a theoretical building is viewed as sufficiently high when the infiltration rate is indicated as a parameter.

3.4. Solar thermal system, auxiliary heater and cooling tower model

The TRNSYS model of the solar thermal system including the storage tank is based on the IEA-SHC-Task 32 TRNSYS deck file [19]. The collector loop is connected to a heat exchanger that feeds into a storage tank. The auxiliary heater is a simple electric water heater that is placed in the feed water from the storage tank and heats, if necessary, the water mass flow prior to entering the regenerator of the LDAC system. To simplify the modeling of the cooling tower, it is assumed that the cooling tower can provide cooling water at 3 K above the wet-bulb temperature of the ambient air.

3.5. System control

The LDAC system for the annual system simulations is controlled by a PI controller to not exceed the set-point humidity ratio of 6 g_w/kg_{da}. The

[1] Gebäudeenergiegesetz vom 8. August 2020 (BGBl. I S. 1728).

controller reflects a capacity control of the LDAC unit. It regulates the mass flow rates of all fluid streams evenly by a single factor between 0.1 and 1. A factor of 1 corresponds to each design value, lower values are used for partial load. When reducing the mass flow rate of the liquid desiccant down to 0.1 of the design value, attention must be paid to ensure proper wetting of the wicking fins in practical implementation. When the system is running and the humidity ratio drops below the set-point of 6 g_w/kg_{da} at the lowest capacity of 0.1, the system keeps running until a humidity ratio of 5.5 g_w/kg_{da} is reached, to avoid excessive cycling (by using a differential controller with hysteresis). Besides the PI controller for the mass flow rates there is a PID controller that regulates the auxiliary heater and therewith the temperature of the heating water for regeneration. This PID controller acts if the LDAC unit is running at a high rate of over 0.7 and provides the auxiliary heater with a target temperature between 40 °C and 80 °C for regeneration. The auxiliary heater raises the heating water temperature coming from the storage tank to the target temperature, if necessary. Both (simulated) PID controllers were tuned based on the method of Ziegler and Nichols [20]. The tuning values used in the simulation are shown in Table 4. Tuning values for real PID controllers might differ from the ones used in the simulation due to the simulated timestep of 30 s for the annual system simulation. An example of employing a PID controller for volume flow control can be found in [21]. The pump of the solar loop will turn on as soon as the temperature in the collector is higher than the temperature at the bottom of the storage tank.

4. Comparison of modeled and measured data of the LDAC unit

In this section, measured and modeled results of the LDAC unit are presented that are carried out for a six-hour period with constant inlet air conditions and for a six-day period with variable inlet air conditions emulating weather data for Stuttgart, Germany. The six-day measurements are carried out twice, first for adiabatic absorber conditions (without internal cooling of the absorber) and then with internal cooling.

4.1. Evaluation procedure

The moisture removal rate, $\dot{m}_v$ of the absorber is calculated from both, air and liquid desiccant (solution) side, as described by eq. (8) and eq. (9):

$$\dot{m}_{v,\,a} = \dot{m}_{da} \cdot (x_{out} - x_{in}) \tag{8}$$

$$\dot{m}_{v,\,sol.} = \dot{m}_{salt} \cdot (X_{out} - X_{in}) \;\text{ with }\; X = \frac{1-\xi}{\xi} \tag{9}$$

With $\dot{m}_{da}$ as the mass flow rate of the dry air. The transferred vapor mass flow rate in the regenerator is called humidification rate and is calculated in the same manner as the moisture removal rate of the absorber. To evaluate the plausibility of the measurements, a mass balance factor and energy balance factor, κ_m and κ_e are defined according to eq. (10) and eq. (11), respectively for the absorber and the regenerator.

$$\kappa_m = \frac{\dot{m}_{v,\,a}}{\dot{m}_{v,\,sol}} \tag{10}$$

Table 4
Controller parameters.

Controller	Range	Gain Constant	Integral Time	Derivative Time
Capacity (volume flow) controller	0.1 … 1	$-5 \cdot 10^3$	20 min	0
Auxiliary heater controller	40 … 80 °C	$-3 \cdot 10^6$	200 min	2.4 min

$$\kappa_e = \frac{\dot{H}_{sorp}}{\dot{Q}_{a,sens} + \dot{Q}_{sol} + \dot{Q}_w} \tag{11}$$

The deviation of the evaluated values from 1 is a quality measure of the experiments. $\dot{H}_{sorp}$ is the sum of evaporation and dilution enthalpy flow. The average absolute deviation (AAD) and the percentage average absolute deviation (AAD%) for any evaluated variable P between the experimental and the simulation results, are defined as:

$$\mathrm{AAD}(P) = \frac{1}{n} \cdot \sum |P_{sim} - P_{meas}| \tag{12}$$

$$\mathrm{AAD\%}(P) = \frac{1}{n} \cdot \left(\frac{\sum |P_{sim} - P_{meas}|}{\sum P_{meas}} \right) \cdot 100\% \tag{13}$$

The AAD% of the moisture removal and humidification rates and the AAD for temperature change of the fluids are evaluated.

4.2. Measurement results of an internally cooled absorption process with constant inlet conditions (six-hour period)

The heat sources and sinks for the LDAC system for internal heating and cooling of the sorption processes and for pre-conditioning of the inlet air are emulated by water and air conditioning units in the laboratory. The set-point inlet variables of the LDAC unit six-hour measurements are shown in Table 5.

The mass balance and energy balance factors κ_m and κ_e for this measurement are: 0.85 and 1.02 for the absorption process and 0.92 and 0.96 for the regeneration process. Fig. 2 shows the temperature and humidity ratio at the internally cooled absorber inlet and the internally heated regenerator inlet. While the values of the inlet temperatures of the two components differ only slightly from each other, the values of the humidity ratio differ by about 2 g_w/kg_{da} due to stratification of the inlet air during pre-conditioning.

Fig. 3 shows measured as well as simulated moisture removal rates of the air flow in the absorber and the humidification rates of the air flow in the regenerator, $\dot{m}_v$. The measured and the simulated curves are almost parallel after about 30 min, and they slowly approach one another. Thus, the model depicts the dynamic behavior of the LDAC system well after the start-up phase. The percentage average absolute deviation between the measured and simulated values after 1 h (in the period 1 h $< t <$ 6 h) is about 5 % for the absorption and 12 % for the regeneration process. However, the measurement accuracy of the latter was poor due to inappropriate positioning of the temperature sensor of the outlet air. The temperature as well as the relative humidity sensors were installed after the air ventilator behind the regenerator. This resulted in a change of air temperature due to the ventilator that influenced the measured value. The uncertainty of the measured moisture removal rate of the absorber is about ± 11 % and of the humidification rate of the regenerator is about ± 12 %. These uncertainties are the average values of the last 30 min of each measurement calculated according to uncertainty propagation of the equation (8).

The measured and simulated air temperature difference between in- and outlet of the absorber and regenerator is shown in Fig. 4. The average absolute deviations between the calculated and measured values are about 0.7 K in the absorber and 0.9 K in the regenerator (for 1 h $< t <$ 6 h). The uncertainty of the measured change of the air temperature is about ± 0.7 K. Fig. 5 shows the measured and simulated difference between water in- and outlet temperatures for the absorber

Table 5
Average values of the inlet conditions of the six-hour measurement.

	$\dot{m}_{a,in}$ kg/h	$T_{a,in}$ °C	$x_{a,in}$ g_w/kg_{da}	$\dot{m}_{sol,in}$ kg/h	$\dot{m}_{w,in}$ kg/h	$T_{w,in}$ °C
Regenerator	355	24.5	12.0	228	985	60
Absorber	1188	24.9	14.1	323	1998	25

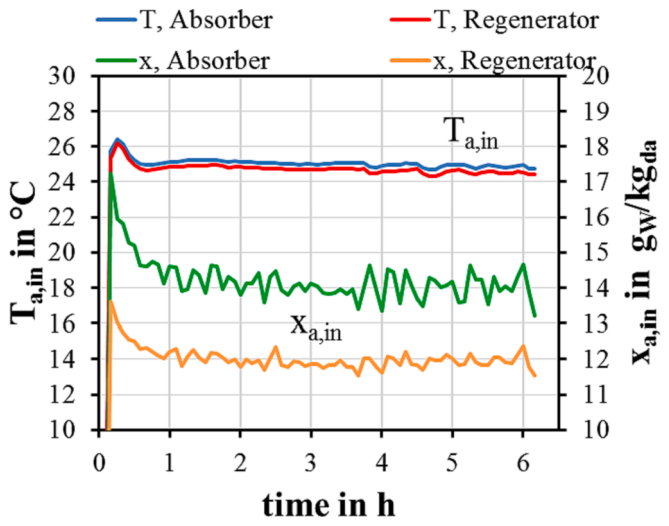

Fig. 2. Measured inlet air temperatures and humidity ratios at the internally cooled absorber and the regenerator during six-hour measurement.

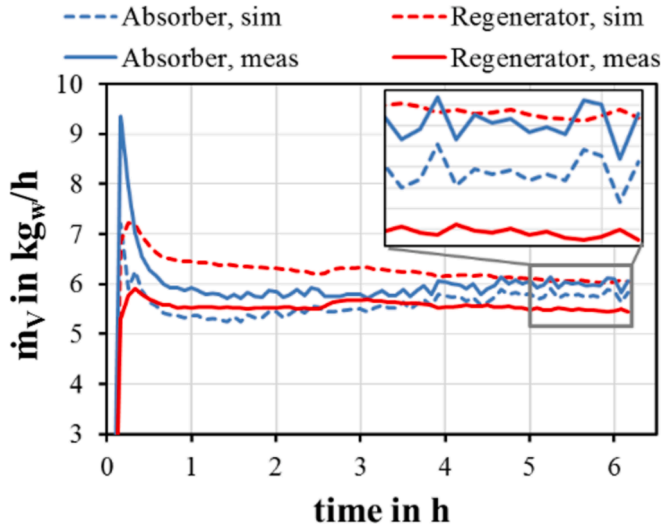

Fig. 3. Measured and simulated moisture removal rate in the internally cooled absorber and humidification rate in the regenerator during six-hour measurement.

and regenerator. The accordance between measured and calculated values is very well. The average absolute deviation is less than 0.2 K for both, absorber and regenerator (for 1 h < t < 6 h).

Compared to typical accuracies reached for heat and mass transfer models for liquid desiccant systems, the accuracy for the moisture removal rate $\dot{m}_v$ is very high, especially when considering that the heat and mass transfer coefficients are modelled solely with standard correlations and without any parameter fit. A percentage average absolute deviation of the vapor mass flow rate in the absorber of only 5 % for the six-hour measurements is reached with the model presented in this work. Also, the heat transfer between the three fluids is modelled very precisely, shown in the accuracy of simulating the measured air temperatures.

4.3. Measurements with emulated outdoor conditions of a six-day period

The LDAC unit model is validated with two six-day measurements for dynamic inlet conditions, one with internal cooling and the other one with an adiabatic absorption process. Table 6 shows the average

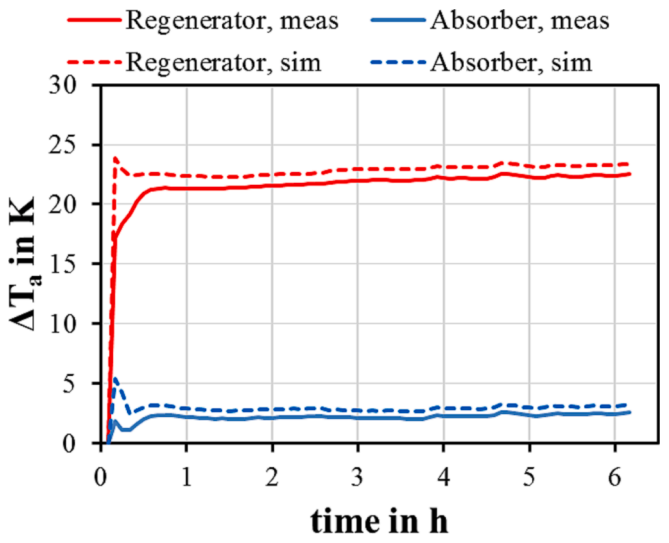

Fig. 4. Measured and simulated difference between air in- and outlet temperatures for the absorber and regenerator during six-hour measurement.

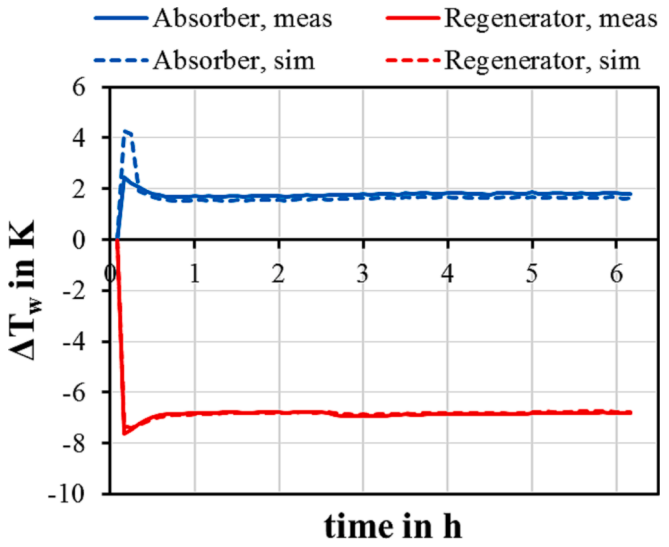

Fig. 5. Measured and simulated difference of water in- and outlet temperatures for the absorber and regenerator during six-hour measurement.

Table 6
Average values of the inlet conditions of the transient six-day measurement.

	$\dot{m}_{a,in}$ kg/h	$\dot{m}_{sol,in}$ kg/h	$\dot{m}_{w,in}$ kg/h	$T_{w,in}$ °C
Regenerator	360	237	1002	60
Absorber	1190	304	2000	25

absolute values of the flow rates and hot water inlet temperature for the measurements. The air inlet temperature and humidity ratio profiles used in both measurements are shown in Fig. 6.

The air inlet temperature varies in a sinus-like six-day profile with a maximum temperature of approx. 30 °C and a minimum temperature of 11 °C. The amplitude of the humidity ratio between day and night is much smaller than that of the air temperature. Due to the stratification in the air duct, the humidity ratio at the inlet of the absorber is significantly higher than that of the regenerator with a deviation of about 1–2 g_w/kg_{da}. During the six-day period, the inlet humidity ratio of the absorber decreases from approx. 14 g_w/kg_{da} to approximately 6 g_w/kg_{da}

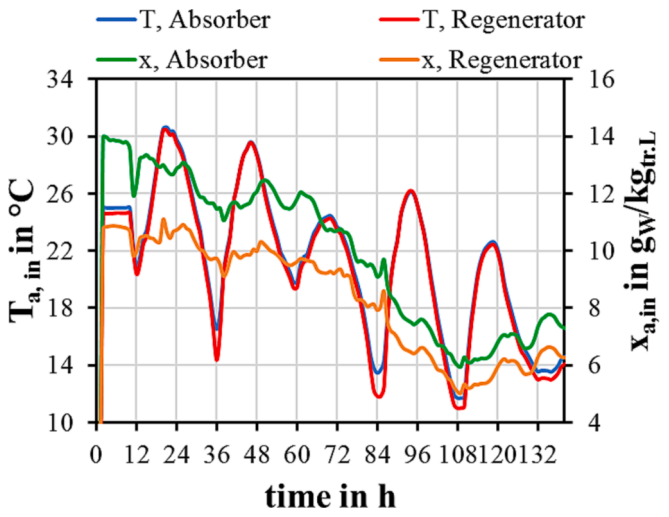

Fig. 6. Measured inlet air temperature and humidity ratios at the absorber and regenerator during six-days measurements.

after about 4.5 days. Therewith, the measurements cover a wide range of inlet humidity ratios.

4.4. Results for the internally cooled absorption process with dynamic ambient air conditions

Fig. 7 shows the moisture removal rate of the air flow in the absorber and the humidification rate of the air flow in the regenerator, $\dot{m}_v$, evaluated from the measurements and simulations. The two curves at the bottom show the deviations between measured and calculated values (referred to the right axis). The trend of the curves for the measured and calculated values agree well also for the internally cooled absorption and the regeneration process. The percentage average absolute deviation between the measured and calculated values of the moisture removal rate of the internally cooled absorption process yields 6 % and the percentage average absolute deviation of the humidification rate in the regenerator yields 7 %. Therewith, the deviations increase only very slightly, by 1 percent point (from 5 to 6 %), for the measurement with dynamic inlet conditions compared to constant inlet conditions.

The average deviation between the measured and calculated air-temperature rise is 0.3 K in the internally cooled absorber and the heating-water temperature drop in the regenerator is 0.1 K (Fig. 8).

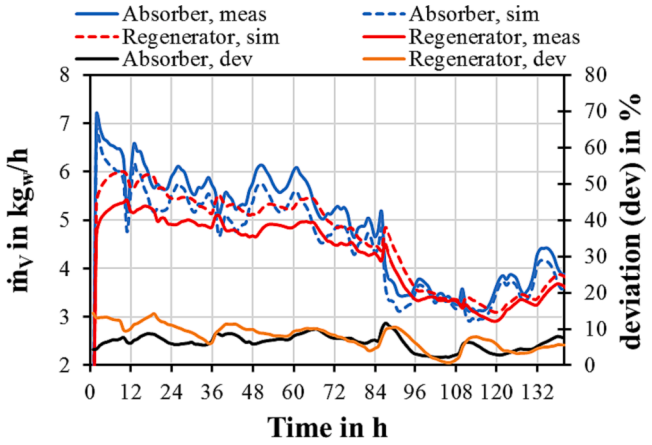

Fig. 7. Measured and simulated moisture removal rate of the air in the internally cooled absorber and humidification rate in the regenerator with the corresponding deviations over the time.

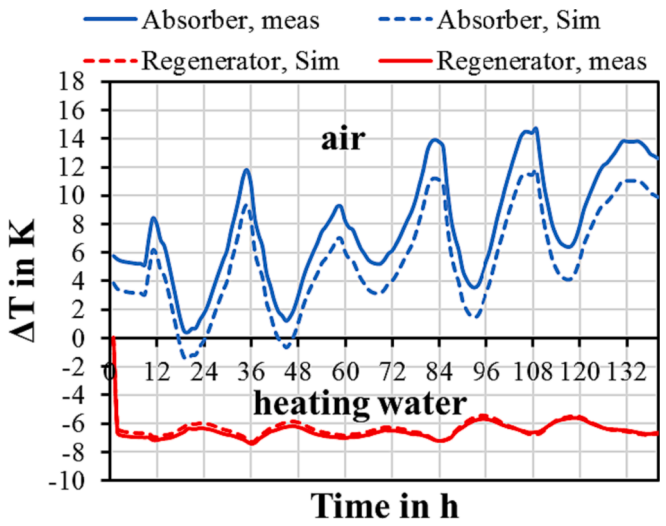

Fig. 8. Measured and simulated air (absorber) and heating water (regenerator) temperature difference over the time.

Thus, despite of the dynamic inlet conditions, the values are within the measurement accuracy, and it can be concluded that the modelling of the heat transfer is very precise.

4.5. Results for the adiabatic absorption process with dynamic ambient air conditions

Fig. 9 shows the moisture removal and humidification rates analog to Fig. 7. Compared to the six-day internally cooled absorption process, in the adiabatic process the simulation results yield a decrease of the moisture removal rate of about 18 %, the measurements yield a decrease of about 15 %.

Similar to the internally cooled process, the calculated trends of the moisture removal rates agree well with the measured ones for both, the absorption and regeneration process. The percentage average absolute deviation between calculated and measured values of the moisture removal rate yields 8 % for the adiabatic absorption process and 10 % for the regeneration process (Fig. 9, right axis). Thus, compared to the internally cooled absorptions process, the accuracy of the modeled moisture removal rate of the adiabatic operation is reduced. The

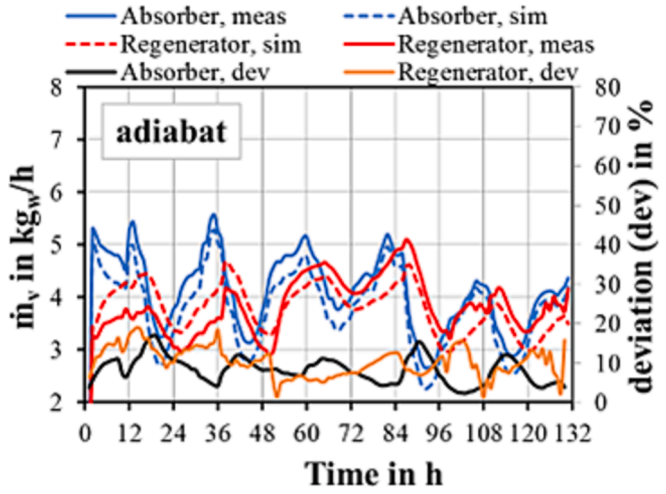

Fig. 9. Measured and simulated moisture removal rate of the air in the absorber (adiabatic process) and humidification rate of the air in the regenerator over the time. The curves at the bottom show the deviations between measured and calculated values.

percentage average absolute deviation of the moisture removal rate of the adiabatic absorption process increases from 6 to 8 %. For the internally cooled operation, the curves are smoother. Moreover, the absolute values of $\dot{m}_v$ are lower for the adiabatic process, which leads to a smaller relative measurement accuracy. Additionally, a dependency between the model accuracy and the inlet air temperature can be observed for the adiabatic system. The deviation of the moisture removal rate in the absorber increases with higher inlet air temperatures, while the deviation of the humidification rate in the regenerator increases with sinking inlet air temperatures as seen in Fig. 9, when considering the input conditions in Fig. 6. This behavior was not visible for the system with the internally cooled absorber.

The model results for the temperature changes are very precise for both operating conditions. As shown in Fig. 10, the average absolute deviation between the measured and calculated temperature rise of the air in the adiabatic absorber is 0.4 K (blue lines) and the deviation of the heating-water temperature drop is 0.1 K (red lines).

It can be concluded that the accuracy of the system model presented in this paper is similar to the values reported by Crofoot [10], while it does not require detailed information of heat and mass transfer coefficients to be evaluated as model parameter. The deviation between simulated and measured values are within the measurement accuracy. This means that a well-suited model was developed that uses only well-known correlations, geometric parameters, physical as well as chemical properties. The transport properties are calculated dynamically based on the input conditions. This model is independent of any parameter that needs to be fitted with measurements. Therefore, the applicability of this model to other LDAC systems should be high but could only be verified for this one LDAC unit so far. Further improvements of the model could be implemented by accounting for impartial wetting of the wicking fins which was not considered in this model but can greatly influence the performance of the LDAC unit.

5. Annual system simulation results

5.1. Heat load and solar irradiance

The heat load for the regeneration can be calculated based on the dehumidification load and the regenerator specific heat input (RSHI) which describes the heat input into the regenerator per absorbed water mass in the absorber (eq. (14)).

$$\mathrm{RSHI} = \frac{\dot{Q}_{\mathrm{reg}}}{\dot{m}_{\mathrm{v,abs}}} \tag{14}$$

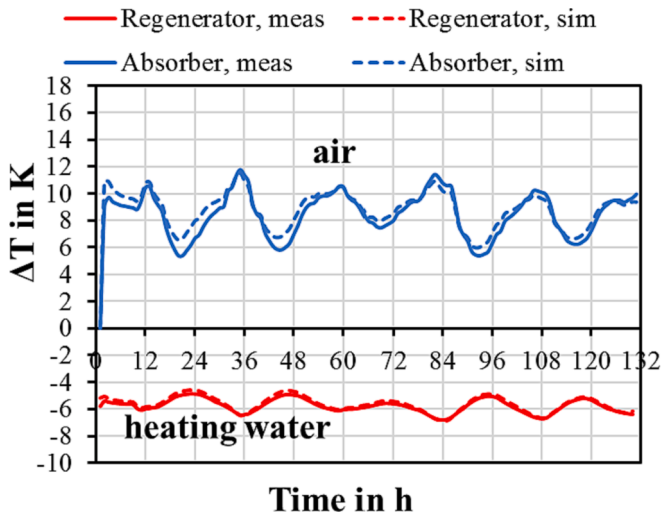

Fig. 10. Measured and simulated air temperature rise in the absorber and heating water temperature drop in the regenerator over the time.

For the investigated building, the infiltration of ambient air is the sole load of humidity. Using the difference between the ambient air humidity ratio x_{amb} and the set-point humidity ratio x_{set} the mass flow of water vapor $\dot{m}_{\mathrm{v,inf}}$ into the building through infiltration can be calculated according to eq. (15).

$$\dot{m}_{\mathrm{v,inf}} = (x_{\mathrm{amb}} - x_{\mathrm{set}}) \cdot V_{\mathrm{a}} \cdot \rho_{\mathrm{a}} \cdot n_{\mathrm{inf}} \cdot \frac{\mathrm{h}}{3600\mathrm{s}} \tag{15}$$

V_{a} is the air volume inside the building with a density of ρ_{a}. All positive values of the infiltration water vapor mass flow rate $\dot{m}_{\mathrm{v,inf}}$ can be considered a dehumidification load and needs to be removed in the absorber of the LDAC system to reach the set-point humidity ratio inside the building. The correlation between infiltration rate and dehumidification load is proportional to the air volume of the building V_{a} as seen in eq. (15). Furthermore, the correlation is influenced by the set-point humidity ratio and the ambient conditions. Assuming a constant RSHI of 7000 kJ/kg, based on experimental data, and a set humidity ratio of 6 g_w/kg_{da} the total regeneration heat load can be calculated using eq. (14), eq. (15) with the ambient weather data for Kassel. Mean temperature and humidity values are shown in Fig. 11. The calculated regeneration heat load is used for dimensioning of a solar thermal system. The regeneration heat load in relation to the infiltration rate is shown in Fig. 12. The heat demand for dehumidification occurs predominantly during the summer months and therefore shows a good correlation to the course of solar irradiance as shown in Fig. 12.

5.2. Dimensioning of the solar thermal system

Typical dimensioning for solar process heat is based on the VDI 3988 [22] to achieve full solar coverage of the heat demand on a good summer day and thereby avoid solar surpluses. In contrast to most solar applications this kind of dimensioning still generates solar surpluses for the considered application, which unavoidably occur during winter months because the heat demand drops to zero. For this investigation the solar thermal system (collector area A_{coll} and storage volume V_{st}) is dimensioned for summer days with high irradiance of more than 6 kWh/(m^2d). Of the corresponding daily heat demands the 0.85 quantile is used for dimensioning of the solar system. This way the heat demand on days with high irradiance can mostly be covered. Table 7 shows the resulting size of the solar thermal system based on this deduction of the daily heat demand for a good summer day and following the guidelines in VDI 3988 [22]. Additionally, simulations are carried out with the size of the solar system increased and decreased by 50 %, respectively, as shown in Table 7. This includes a resizing of the collector area A_{coll} as well as the volume of the solar water storage tank V_{st}. The simulated LDAC unit remains the same throughout the parameter variation.

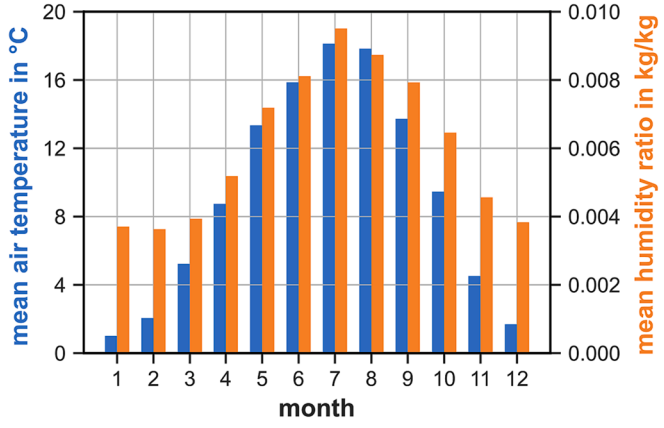

Fig. 11. Monthly mean temperature and mean humidity ratio in Kassel, Germany.

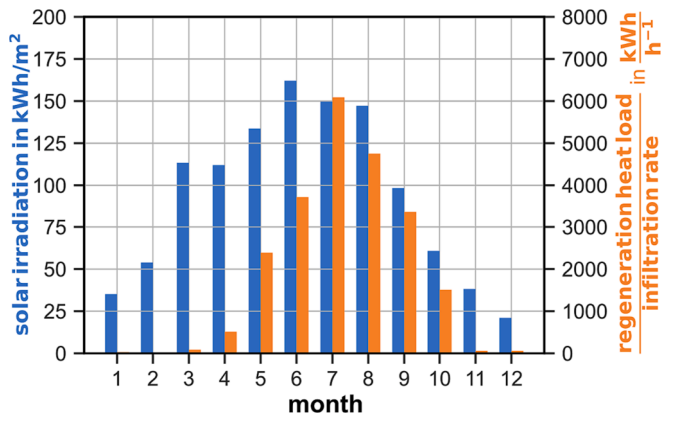

Fig. 12. Monthly solar irradiation on a tilted surface (30°) and monthly heat load of regeneration per infiltration rate; set humidity ratio: 6 g_w/kg_{da}.

Table 7
Investigated infiltration rates with the corresponding size of the solar thermal system.

Infiltration rate	Daily Heat Demand (0.85 quantile)	VDI		VDI + 50 %		VDI – 50 %	
		A_{coll}	V_{st}	A_{coll}	V_{st}	A_{coll}	V_{st}
h^{-1}	kWh	m^2	m^3	m^2	m^3	m^2	m^3
0.1	22.1	7	1	10.5	1.5	3.5	0.5
0.3	66.3	22	3	33	4.5	11	1.5
0.5	110.5	38	4	57	6	19	2
0.7	154.7	53	6	79.5	9	26.5	3

5.3. *Impact of infiltration rates and of the dimension of the solar heating system*

The effectiveness of the solar assisted LDAC system in maintaining the desired humidity level is shown in Fig. 13. It shows the sorted annual humidity inside the simulated building (for the most humid 5000 h). The control effect is clearly visible with almost straight lines at 6 g_w/kg_{da} for around 1000 h up to over 3000 h of the year. For lower infiltration rates such as 0.1 h^{-1}, the control effect of the differential controller that keeps the LDAC system running at the lowest rate of 0.1 until a humidity ratio of 5.5 g_w/kg_{da} is reached plays a greater role, reducing the active time of the PID controllers to maintain 6 g_w/kg_{da} and increasing the time where the humidity is between 6 g_w/kg_{da} and 5.5 g_w/kg_{da}. At the high humidity end of the graph, transgressions of the set humidity ratio can be seen.

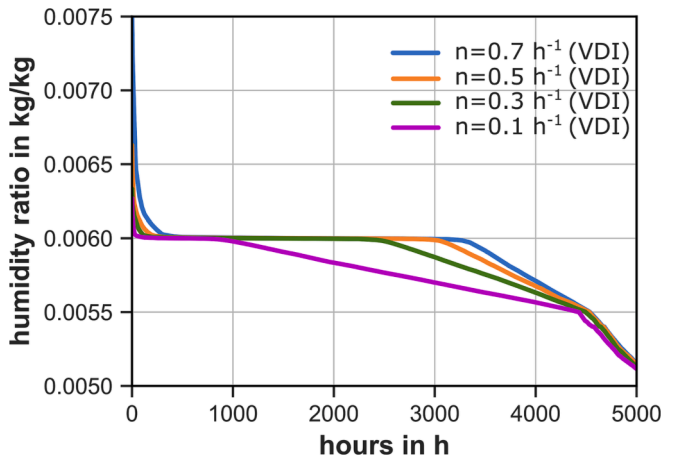

Fig. 13. Sorted resulting humidity ratio inside the building with the employed solar assisted LDAC system and its control with different infiltration rates.

They occur at extreme outdoor ambient conditions with the highest humidity ratio and represent times when the LDAC system is temporarily not able to completely meet the dehumidification load for high infiltration rates.

The solar fraction f_{solar} is defined as the heat provided by the solar thermal system divided by the total energy provided by the solar thermal system and the auxiliary heater (eq. (16)):

$$f_{solar} = \frac{Q_{solar}}{Q_{solar} + Q_{aux}} \tag{16}$$

Q_{solar} is calculated as the total heat provided by the solar system into the storage tank, while Q_{aux} is the total heat added to the passing fluid in the auxiliary flow through heater.

Fig. 14 shows the annual solar fraction f_{solar} for the different collector areas and storage volumes as shown in Tab. 7 with a LDAC system as shown in Fig. 1. The dimensioning based on the VDI shows high solar fractions between 70 % for an infiltration rate of 0.1 h^{-1} and 81 % for an infiltration rate of 0.5 h^{-1}. By increasing the size of the solar system by 50 %, the solar fraction increases by 10 up to 19 percent points. Decreasing the solar system size by 50 % leads to solar fractions of 39 % for a low infiltration rate and up to 53 % for an infiltration rate of 0.7 h^{-1}.

Increasing the size of the solar system leads to more solar surpluses, thus decreasing the area-specific solar yield q_{coll} of the collector as shown in Fig. 15.

$$q_{coll} = \frac{Q_{solar}}{A_{coll}} \tag{17}$$

The solar yield not only decreases with the collector sizing, but also with the infiltration rate. To achieve higher dehumidification capacity the LDAC system requires higher regeneration temperatures. This decreases the collector efficiency and increases the auxiliary heat to raise the temperature from the storage tank to the necessary level.

Fig. 16 shows the comparison of a LDAC system with an internally cooled and an adiabatic absorber, both with the same solar thermal system size based on the VDI. Without the cooling tower the solar fraction decreases between 7 and 12 percent points for the otherwise identical system configuration and the same simulation parameters. The solar yield is unchanged with or without the cooling tower, but the auxiliary heater needs to provide more heat, because the dehumidification process is running less efficiently (higher RSHI) if not cooled, as shown in Fig. 17. The RSHI for the internally cooled absorption process is between 12 % and 20 % lower than for the adiabatic absorption process. The cooling water for the internally cooled absorber represents an additional input to drive the process, which is not accounted for in

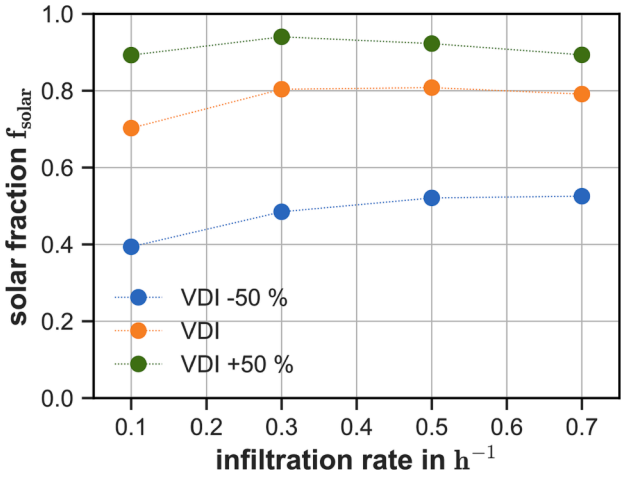

Fig. 14. Annual solar fraction for different infiltration rates and different solar thermal system sizes.

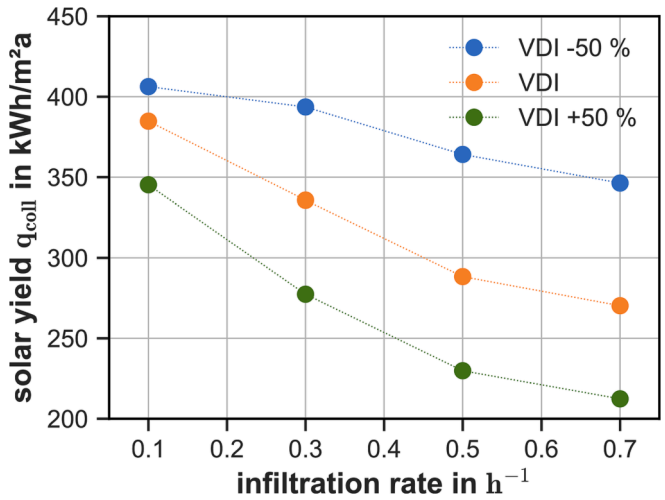

Fig. 15. Annual specific solar yield for different infiltration rates and different solar thermal system sizes.

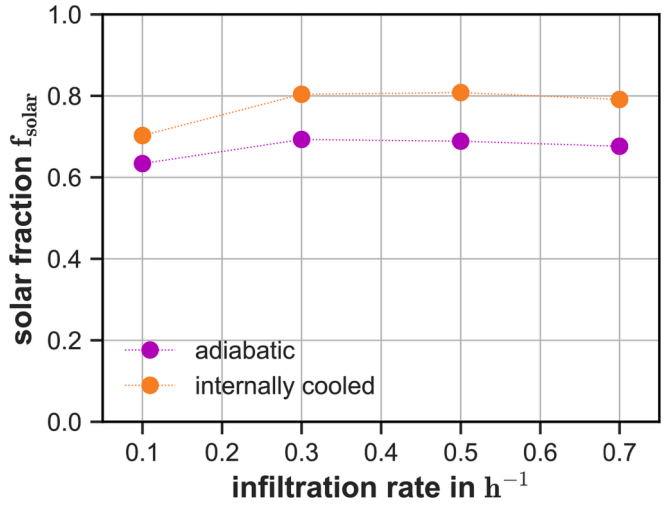

Fig. 16. Annual solar fraction for an internally cooled and an adiabatic absorber for different infiltration rates.

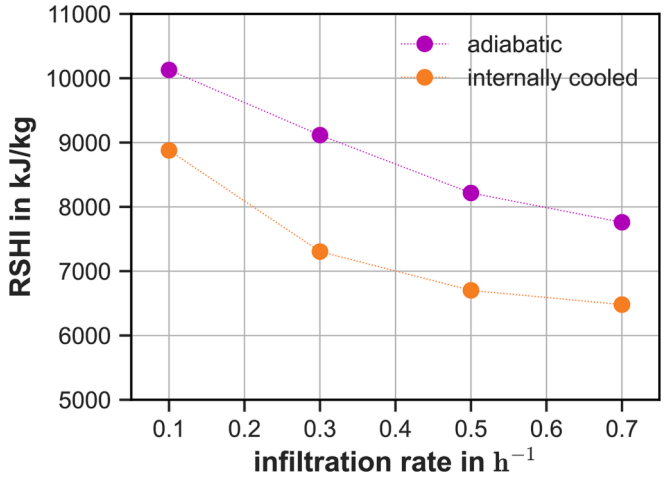

Fig. 17. Annual regenerator specific heat input (RSHI) for an internally cooled and an adiabatic absorber for different infiltration rates.

the RSHI. The RSHI also decreases with increasing infiltration rate for this investigation. For high infiltration rates, the auxiliary heater often increases the regeneration temperature drastically to meet the peak load of the dehumidification. For low infiltration rates, the LDAC unit is running mostly in part load. The auxiliary heater is often employed to keep the minimum regeneration temperature of 40 °C. Therefore, the regeneration temperature is mostly higher in the simulations with high infiltration rate. Higher regeneration temperatures increase the energy efficiency and therefore decrease the RSHI.

6. Conclusion

A TRNSYS model of a liquid desiccant air conditioning system to dehumidify indoor air is developed and validated with measurements. The determined accuracies of the system model show that the model describes the steady-state and dynamic operating characteristics of the LDAC-unit in a suitable manner. In opposite to most models presented in the literature, the presented model describes the heat and mass transfer correlations with solely geometric as well as physical and chemical properties and is therefore independent of measured values. Moreover, it includes a liquid desiccant storage tank and describes transient conditions with an average absolute deviation between measured and calculated values of the moisture removal rate of about 6 % for a period of 6 days with ambient air conditions and an internally cooled absorption process.

Having the infiltration into a building as a main source of humidity leads to a high correlation between the irradiance and the dehumidification load. Sizing the solar system based on full solar coverage on a good summer day yields high solar fractions between 70 % and 81 %. Solar fractions up to 94 % can be reached if the collector size is increased by 50 % of the initial sizing.

The use of a cooling tower to internally cool the absorption process increases the efficiency by decreasing the RSHI of the LDAC system by 12 to 20 % and thereby increases the solar fraction by about 10 percent points versus a system with an adiabatic absorber.

CRediT authorship contribution statement

Wael Mandow: Conceptualization, Methodology, Investigation, Writing – original draft, Validation, Software. **Felix Micus:** Methodology, Writing – original draft, Writing – review & editing, Software. **Lisa Völker:** Conceptualization, Writing – review & editing. **Daniel Fleig:** Resources, Writing – review & editing, Project administration. **Ulrike Jordan:** Conceptualization, Methodology, Writing – review & editing, Supervision, Funding acquisition.

Declaration of competing interest

The authors declare the following financial interests/personal relationships which may be considered as potential competing interests: Wael Mandow reports financial support was provided by German Federal Environmental Foundation. Lisa Voelker reports financial support was provided by IWB-EFRE Programm Hessen.

Data availability

Data will be made available on request.

Acknowledgements

The research project was financed by the German Federal Environmental Foundation (DBU) with a PhD scholarship and by the IWB-EFRE (European Regional Development Fund)-Programm Hessen (Project title: LDAC-Anlagen, EF960 0017/2019 20005248). The authors would like to express their sincere thanks for the support.

References

[1] X. Chen, S. Riffat, H. Bai, X. Zheng, D. Reay, Recent progress in liquid desiccant dehumidification and air-conditioning: A review, Energy and Built, Environ. 1 (2020) 106–130, https://doi.org/10.1016/j.enbenv.2019.09.001.

[2] A.T. Mohammad, S.B. Mat, K. Sopian, A.A. Al-abidi, Review: Survey of the control strategy of liquid desiccant systems, Renew. Sustain. Energy Rev. 58 (2016) 250–258, https://doi.org/10.1016/j.rser.2015.12.333.

[3] Q. Ronghui, L. Lin, H. Yu, Energy performance of solar-assisted liquid desiccant air-conditioning system for commercial building in main climate zones, Energ. Conver. Manage. 88 (2014) 749–757, https://doi.org/10.1016/j.enconman.2014.09.006.

[4] E. Kozubal, L. Herrmann, M. Deru, J. Clark, A. Lowenstein, Low-Flow Liquid Desiccant Air-Conditioning: Demonstrated Performance and Cost Implications, 2014. https://doi.org/10.2172/1159373.

[5] X. Liu, B. Guan, X. Liu, Experimental Study on the Filtration Efficiency of Structured Packing Air Handling Processors, Procedia Eng. 121 (2015) 2037–2043, https://doi.org/10.1016/j.proeng.2015.09.204.

[6] J.-Y. Park, D.-S. Yoon, S. Li, J. Park, J.-I. Bang, M. Sung, J.-W. Jeong, Empirical analysis of indoor air quality enhancement potential in a liquid-desiccant assisted air conditioning system, Build. Environ. 121 (2017) 11–25, https://doi.org/10.1016/j.buildenv.2017.05.011.

[7] Experimental Evaluation of a Novel Tube Bundle Solar Driven Liquid Desiccant Regenerator 19 (2014) 1–10.

[8] E. Yohana, M. Endy Yulianto, S. Bahar, A. Alifa Muhammad, N. Laura Indrayani, A study of tea leaves drying using dehumidification process and regeneration of liquid desiccant in a closed-cycle dehumidification-humidification, MATEC Web of Conferences 159 (2018) 2025, https://doi.org/10.1051/matecconf/201815902025.

[9] K. Khouzam, Developing a Solar Drying Machine for Agricultural Products, Rural Research and Development Corporation, no. 09/026, 2009.

[10] L. Crofoot, Experimental evaluation and modeling of a solar liquid desiccant air conditioner, Library and Archives Canada, Ottawa, 2012.

[11] A.K. Mohaisen, Z. Ma, Development and modelling of a solar assisted liquid desiccant dehumidification air-conditioning system, Build. Simul. 8 (2015) 123–135, https://doi.org/10.1007/s12273-014-0196-1.

[12] T. Zhang, X. Liu, J. Jiang, X. Chang, Y. Jiang, Experimental analysis of an internally-cooled liquid desiccant dehumidifier, Build. Environ. 63 (2013) 1–10, https://doi.org/10.1016/j.buildenv.2013.01.007.

[13] Z. Yang, M. Qu, K.R. Gluesenkamp, O. Abdelaziz, Liquid Desiccant System Component Models in the Sorption System Simulation Program (SorpSim). In: Proceedings of 12Th IEA Heat Pump Conference, 2017.

[14] A. Coca-Ortegón, J. Prieto, A. Coronas, Modelling and dynamic simulation of a hybrid liquid desiccant system regenerated with solar energy, Appl. Therm. Eng. 97 (2016) 109–117, https://doi.org/10.1016/j.applthermaleng.2015.10.149.

[15] S. Bouzenada, C. McNevin, S. Harrison, A. Kaabi, Performance of a liquid desiccant air-conditioner driven by evacuated-tube, flat-plate, or hybrid solar thermal arrays, Energ. Buildings 117 (2016) 53–62, https://doi.org/10.1016/j.enbuild.2016.02.002.

[16] Comparison of Modeled and Measured Heat and Mass Transfer in a Liquid Desiccant Air-Conditioning System 13 (2018) 1–11.

[17] M.R. Conde, Properties of aqueous solutions of lithium and calcium chlorides: formulations for use in air conditioning equipment design, Int. J. Therm. Sci. 43 (2004) 367–382, https://doi.org/10.1016/j.ijthermalsci.2003.09.003.

[18] VDI-Wärmeatlas, Springer Berlin Heidelberg, Berlin, Heidelberg, 2013. https://doi.org/10.1007/978-3-642-19981-3.

[19] Richard Heimrath, Michel Haller, The Reference Heating System, the Template Solar System of Task 32: A Report of IEA Solar Heating and Cooling programme - Task 32, 2007.

[20] J.G. Ziegler, N.B. Nichols, Optimum Settings for Automatic Controllers, J. Fluids Eng. 64 (1942) 759–765, https://doi.org/10.1115/1.4019264.

[21] R.P. Garcia, S.R. Del Oliveira, V.L. Scalon, Thermal efficiency experimental evaluation of solar flat plate collectors when introducing convective barriers, Sol. Energy 182 (2019) 278–285, https://doi.org/10.1016/j.solener.2019.02.048.

[22] Verein deutscher Ingenieure, VDI 3988: Solar thermal process heat, Beuth Verlag GmbH, Berlin, 2020-04-00.